A New Regime of the Agulhas Current Retroflection: Turbulent Choking of Indian–Atlantic leakage

DEWI LE BARS, WILHELMUS P. M. DE RUIJTER, AND HENK A. DIJKSTRA

Institute for Marine and Atmospheric Research Utrecht, Utrecht, Netherlands

(Manuscript received 28 June 2011, in final form 22 February 2012)

ABSTRACT

An analysis of the Indian Ocean circulation and the Agulhas Current retroflection is carried out using a primitive equation model with simplified coastline and flat bottom. Four configurations with 0.25° and 0.1° horizontal resolution and in barotropic and baroclinic cases are considered. The wind stress is taken as control parameter to increase the inertia of the currents. The volume transport of the Indonesian Throughflow, Mozambique Channel, and Agulhas Current are found to increase linearly with the wind stress strength, and three nonlinear retroflection regimes are found. A viscous and an inertial regime had already been documented, but a new turbulent regime appears at large wind stress amplitude. In this turbulent regime, the volume of Agulhas leakage reaches a plateau because of strong mesoscale variability and, in contrast to the other regimes, does not depend on the wind stress magnitude. The physical mechanism causing the plateau is shown to be associated with the cross-jet exchange of Indian Ocean water and water from the Antarctic Circumpolar Current. In the turbulent regime, the permeability of the Agulhas Return Current to material transport increases and the Indian Ocean water available for the Agulhas leakage decreases.

1. Introduction

The gap between the southern tip of Africa and the Subtropical Front (STF) allows a flow of relatively warm and salty water from the Indian Ocean into the Atlantic Ocean, the so-called Agulhas leakage (Gordon 1986). Model simulations (Weijer et al. 2002; Biastoch et al. 2008) suggest that the leakage could impact the strength of the Atlantic Meridional Overturning Circulation (AMOC) and therefore could affect Atlantic climate (Beal et al. 2011). The amount of leakage is the result of complex interactions between the far field [wind stress strength and pattern, Indonesian Throughflow, and stratification] and the local dynamics of the retroflection (De Ruijter et al. 1999). In a region where the eddy kinetic energy (EKE) is among the highest in the world, it is surprising to see that the position of the retroflection is quite stable at interannual time scales (Dencausse et al. 2010).

To understand the controls on the Agulhas leakage many studies focused on the physical mechanisms playing an important role in the retroflection of the Agulhas Current (AC). Looking at steady states in a barotropic model, Dijkstra and De Ruijter (2001) showed the existence of two steady regimes of retroflection depending on the dominant balance in the vorticity equation. For a weak Agulhas Current, friction is dominant, and if the Munk boundary layer is thick enough it is possible to have retroflection due to ''frictional choking.'' When friction decreases, the Agulhas Current becomes stronger and the Munk boundary layer width decreases, leading to an inertial retroflection. In baroclinic models, the gradient of the upper-layer thickness creates positive relative vorticity that strengthens the retroflection (Chassignet and Boudra 1988).

More recently, hindcast simulations of state-of-the-art ocean models were analyzed to investigate the relation between AC transport and leakage. Van Sebille et al. (2009b) found a significant negative correlation between the two quantities, whereas the model used by Rouault et al. (2009) shows a positive correlation. The obvious contradiction between these two studies illustrates the complexity of the processes involved in retroflection and leakage. These hindcast simulations only reproduced a small range of states of the system: for instance, the range of AC transport at 32°S is 61–67 Sv (1 Sv $\equiv 10^6$ m^3 s^{-1}) in Van Sebille et al. (2009b). Moreover, it is not possible

Corresponding author address: Dewi Le Bars, IMAU, Utrecht University, P.O. Box 80.005, 3508 TA Utrecht, Netherlands.
E-mail: d.lebars@uu.nl

DOI: 10.1175/JPO-D-11-0119.1

in those simulations to isolate the effect of the separate mechanisms (e.g., shifts in the wind pattern or variation in the AC transport) on the retroflection (Beal et al. 2011).

For these reasons we designed a systematic series of idealized experiments using a high-resolution model to investigate the relations between wind stress strength, AC transport, position of the retroflection, and leakage. Although a latitudinal shift of the zero wind stress curl line is expected to have an impact on the leakage (De Ruijter et al. 1999), we limit this study to a fixed wind stress pattern with increasing amplitude. We find an interesting transition from the inertial regime to a new turbulent regime of retroflection in which the leakage reaches a limiting plateau value.

In section 2, we present the model, the experiments, and the method used to compute the leakage. In section 3, we analyze the results of the model simulations concerning the Indian Ocean circulation and compare them with those from simple linear models. The retroflection of the AC and the relation with the leakage is investigated in section 4. In section 5, we look at the position of the retroflection and its relation to the AC strength and to the leakage magnitude. The physics of the new retroflection regime is detailed in section 6, and a summary and a discussion of our results appear in section 7.

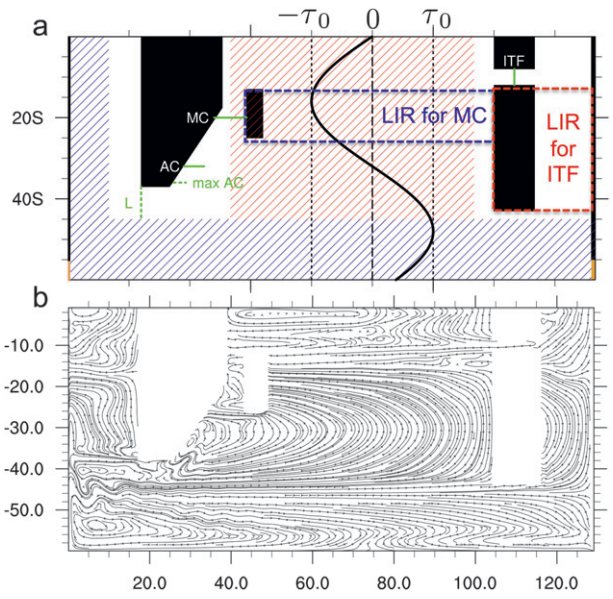

FIG. 1. (a) Model domain with continents (black), ridge (orange), profile of wind stress forcing, and important sections [ITF, MC, AC, and leakage (denoted by L)]. Also indicated are the regions where tracer concentration is fixed to 1 (red hatching) and 0 (blue hatching). The tracer is initialized to zero in the white regions but is free to evolve in time. Dashed contours used to compute the Linear Island Rule (LIR) of Madagascar (blue) and Australia (red) to estimate the MC and the ITF volume transport, respectively, are represented. (b) Transport streamfunction of the upper layer of BC01 under a wind stress of 0.2 N m^{-2}.

2. Model configuration and experiments

a. General setup

In this study, we model the flow in a simplified basin that stretches from 60°S to the equator and from 0° to 130°E (Fig. 1). The domain is centered on the Indian Ocean with the African continent and Madagascar in the western part and the Australian continent in the eastern part. There are three basins in this setup, and we will call them Atlantic Ocean, Indian Ocean, and Pacific Ocean even though the sizes of the Atlantic and Pacific Oceans are much smaller than reality. This setup allows for water to go from the Pacific to the Indian Ocean, which is here referred to as the Indonesian Throughflow (ITF). We use zonal periodic boundary conditions between 60° and 55°S to allow an Antarctic Circumpolar Current to develop. To reduce its intensity, we have added a ridge at 130°E; the longitudinal extent of this ridge is 1° and its height depends on the number of layers of the model. In each case, there is a gap of 500 m between the surface and the top of the ridge. The rest of the domain has a flat bottom.

To study the ocean circulation in this domain, we use the Hallberg Isopycnal Model (HIM; Hallberg 1997). It uses a time-splitting scheme to solve the hydrostatic primitive equations in spherical coordinates on an Arakawa C grid. Four different model configurations were used (see Table 1), with intermediate- [0.25° barotropic (BT025) and baroclinic (BC025)] and high-resolution [0.1° barotropic (BT01) and baroclinic (BC01)] cases. The equilibrium thickness of the top layer in baroclinic models and of the only layer in barotropic models is 1000 m because in the oceans most of the kinetic energy is contained in this layer (Schmitz 1996).

Lateral friction is parameterized with a Laplacian horizontal eddy viscosity. We apply no-slip lateral boundary conditions and no bottom stress. The models are forced by a steady zonal wind stress (Fig. 1a) of the form

$$\tau(\theta) = -\tau_0 \sin\left[\frac{\pi}{32}(\theta - \theta_0)\right], \qquad (1)$$

where θ is the latitude and with $\theta_0 = -32°$. There are two zero wind stress curl lines, one at 16°S and the other one at 48°S. That leaves a gap of approximately 1200 km between the tip of South Africa and the southern zero wind stress curl line. The pattern is fixed but the amplitude of the wind stress is taken as control parameter and ranges from 0.02 to 0.3 N m^{-2}, except for the high-resolution baroclinic model, where the flow for the weakest wind

TABLE 1. Description of the experiments.

Expt	Horizontal resolution	Viscosity ($m^2\ s^{-1}$)	No. of layers	Density ($kg\ m^{-3}$)	Equilibrium thickness of the layers (m)
BT025	0.25°	2000	1	1030	1000
BC025	0.25°	2000	2	1030	1000
				1035	2000
BT01	0.1°	500	1	1030	1000
BC01	0.1°	500	2	1030	1000
				1035	2000

forcing ($\tau = 0.02\ N\ m^{-2}$) was not computed. For each amplitude of the wind stress, we run the model to reach a statistical equilibrium. This takes from a few years for BT025 up to a few decades for BC01. For analysis, we take an average of 5 yr of each experiment for BC01 and an average of 2 yr for the other configurations because the interannual variability is weaker. To compute the EKE and to investigate the impact of eddy rectification on the mean flow, we also run each simulation for an additional year with daily output of velocities instead of monthly.

The choice to take the same wind stress for the easterlies and the westerlies was done to reduce the relative importance of the Antarctic Circumpolar Current that tends to grow very quickly in flat bottom models. In the geographic area considered in this study, average wind stress between 1999 and 2001 from the Scatterometer Climatology of Ocean Winds (SCOW) dataset (Risien and Chelton 2008) based on the data from Quick Scatterometer (QuikSCAT) are approximately $0.05\ N\ m^{-2}$ for the maximum easterlies and $0.2\ N\ m^{-2}$ for the maximum westerlies. These values are part of the forcing used in this study, but direct comparison is not possible because the zonal extent of the Indian Ocean is approximately 10° smaller than reality.

b. Computing the leakage

To compute the leakage of the equilibrium states, we add to the model a passive Eulerian tracer following the same tracer method as Penven et al. (2011). The value of the tracer is fixed to 1 in the Indian Ocean and 0 in the western part of the Atlantic and in the Southern Ocean (Fig. 1a). It is zero initially but can evolve freely in the white regions represented in Fig. 1. An example of snapshot picture is given in Fig. 2a. This tracer is advected with the flow field every two time steps for which a monotonic, conservative tracer advection algorithm (Easter 1993) is used. This passive tracer allows us to follow the Indian Ocean waters south and west of the African continent. The flux of tracer is computed during the simulation and stored as monthly mean. This allows us to take into account the impact of fluctuations on the mean.

To compute the leakage for the flow in a statistical equilibrium, it is important that the concentration of tracer in the retroflection region is constant. We compute the incoming tracer flux through the northern, southern, western, and eastern sections of a box around the retroflection area and make sure the long-term average flux is zero (Fig. 2b). The passive tracer is introduced after spinup of the flow and for all the following analysis we consider states for which both the flow and the tracer concentration have reached a statistical equilibrium. The leakage is computed as the net volume flux of tracer coming from the Indian Ocean that crosses a line at 18°E. It is the net volume flux because, if water from the Indian Ocean retroflects west of 18°E, then it is first counted positive and then negative so it does not add to the leakage. The sensitivity of this measure to the position of the area where it can evolve freely was investigated with two other experiments. First using BC025 with $\tau = 0.2\ N\ m^{-2}$, we move the limit where the tracer concentration is fixed to 0 in the Atlantic from 10° to 5°E; this gives a difference smaller than 2 Sv (approximately 5% of the total leakage). Then, to test the importance of the position of the southern limit, we move it from 45° to 50°S. For BC01 under $\tau = 0.3\ N\ m^{-2}$, the increase of leakage is also around 2 Sv (approximately 7% of the total leakage), which is less than the error E described in section 4. This is because most of the tracer flux that goes south of 45°S is advected to the east by the Antarctic Circumpolar Current.

We also compared the tracer method with the so-called total transport method (Fig. 2c), where the velocities are averaged over 2 yr to smooth the mesoscale structures and we determine the transport of the westward jet south of Africa at 18°E. This total transport method generally overestimates the leakage, mainly because it measures all the water that retroflects west of 18°E as leakage. For all the models, there can be some important differences between the two methods. This shows the need for an advanced method to accurately measure the mean leakage. Another advantage of the tracer method used here is to give a time series of the leakage that allows us to compute the variance and the uncertainty.

3. Transports of the ITF, MC, and AC

In this part, we analyze the time mean volume transport in the ITF, the Mozambique Channel (MC), and the AC (see sections in Fig. 1). We compare the numerical model results with those from the linear island rule (LIR), an analytical model for the transport west of an island (Godfrey 1989), and from the Sverdrup balance. The

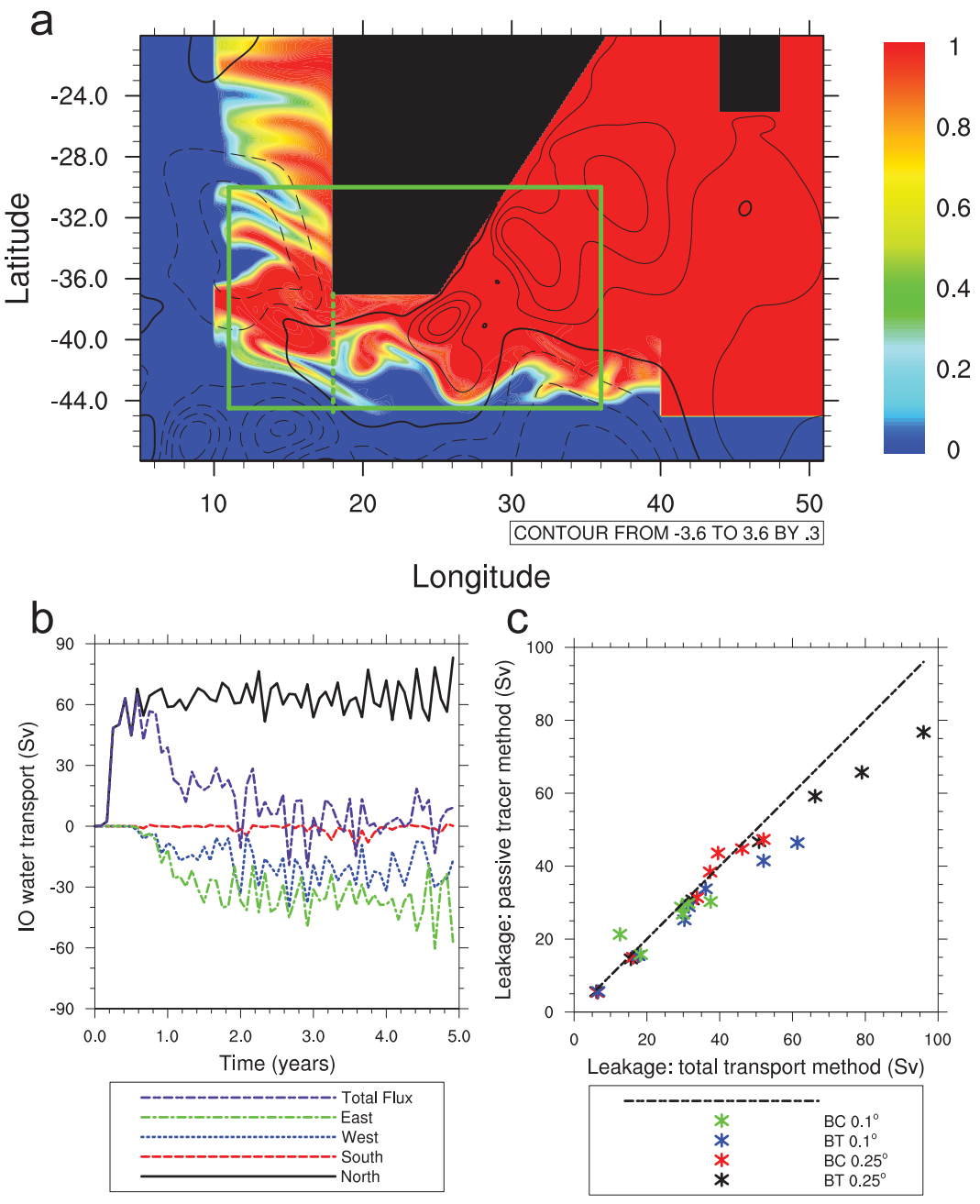

FIG. 2. (a) Snapshot of tracer concentration and sea surface height (contour every 0.3 m) south of Africa during the statistical equilibrium of BC01 forced by a wind stress of 0.2 N m^{-2}. (b) Spinup of the fluxes of tracer at the boundaries of a box [see (a)] for the same model as (a). (c) Comparison of the passive tracer method and the total transport method to compute the leakage.

contours used in the LIR are shown in Fig. 1. For the baroclinic configurations, only the upper-layer transport is considered.

The net transport of the ITF (Fig. 3a) can evolve freely depending, for instance, on the wind stress over the Pacific Ocean. Focus is on the net transport because the flow in the passage is eastward in the north and westward in the south. A flow from the Indian Ocean to the Pacific Ocean is not unrealistic and has been observed from mooring data (Sprintall et al. 2009). However, the net flow is westward for all the model configurations. With the LIR model, we can compute the meridional

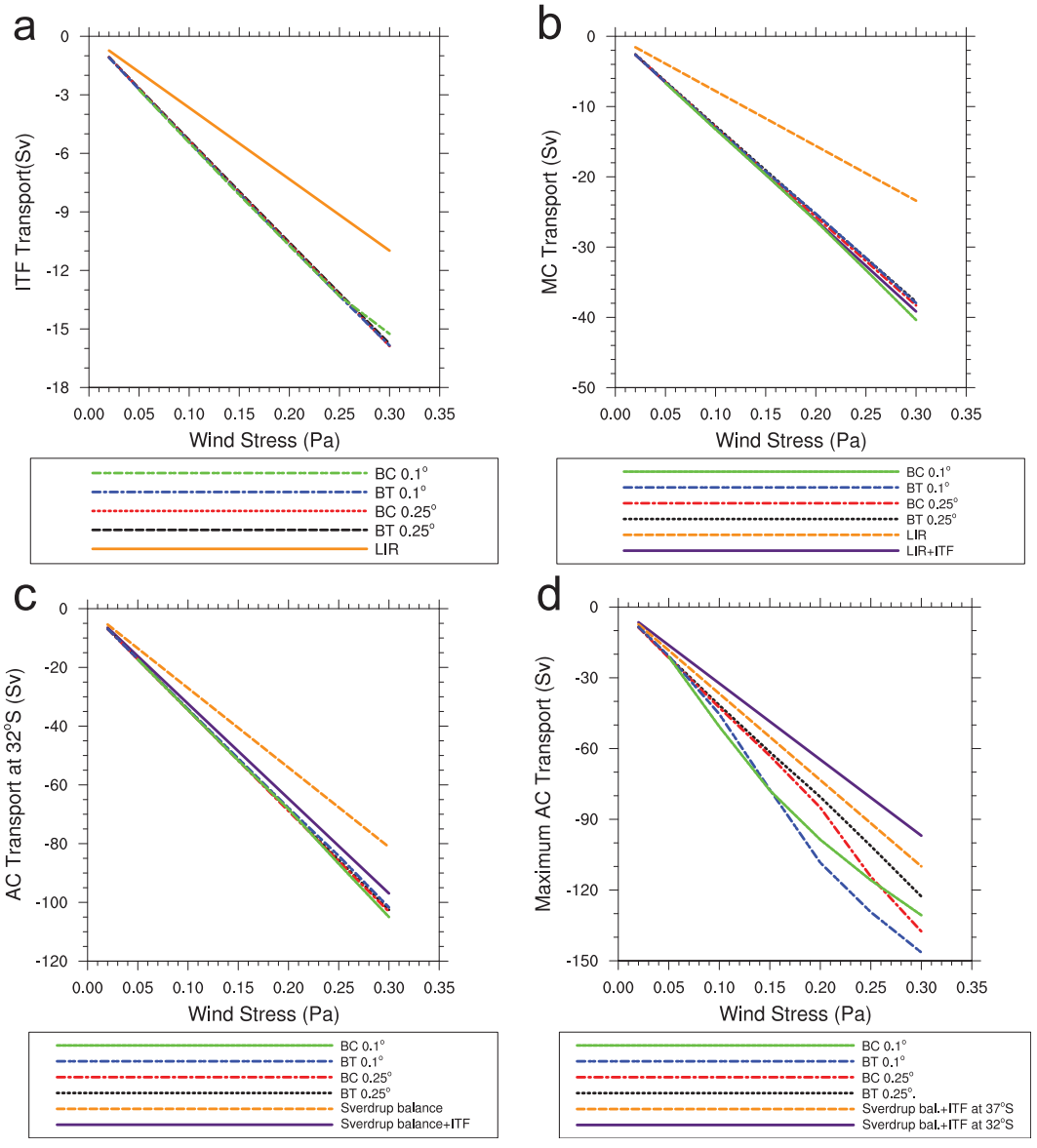

FIG. 3. Transport of (a) ITF, (b) MC, (c) AC at 32°S, and (d) AC at the location where it is maximum (different for each model and wind stress forcing).

transport west of Australia. In a steady state, this transport is equal to the zonal transport in the ITF because of conservation of mass. In the numerical experiments, the transport of the ITF is larger than the LIR estimation (Fig. 3a). This suggests that in these models the ITF transport is the result not only of the wind stress east of Australia but also of an additional input that is independent on the local wind. It is maybe due to the south Indian Ocean gyre that is linked to the Pacific Ocean south of Australia. The MC transport of the numerical models is almost twice the LIR estimation (Fig. 3b). This is because the Indian Ocean basin is not closed in the east. When the net ITF transport is added to the LIR-derived MC transport, then the results are close to the model simulations.

The transport of the AC is more difficult to define than that of the ITF and the MC because the choice of the offshore integration boundary is quite arbitrary and also because it strongly depends on the latitude where it is calculated. When we compute the transport of the AC across a large zonal section spanning 5° (section AC in Fig. 1), then the integration covers the current over the entire recirculation cell and we are able to filter most of the local recirculation effects. The sum of the Sverdrup

and the ITF transport gives a good approximation of the time-mean AC transport of the numerical model results (Fig. 3c).

We also compute the AC transport at the latitude where it is the strongest and integrate the southward velocity from the coast until the point where the velocities turn northward. With this method, the transport does not linearly depend on the wind stress (Fig. 3d) because of the recirculation effects that are nonlinear. The AC transport is then stronger for situations where the inertia is more important. Hence, the relation between the transport of the time-mean currents and the wind stress amplitude is linear, except in the retroflection region.

4. Retroflection regimes of the Agulhas Current

The position and the strength of the AC retroflection are different for each model solution. To characterize the retroflection, we use the nondimensional retroflection index R, defined by

$$R = 1 - \frac{\Phi_L}{\Phi_{\mathrm{AC}}}, \tag{2}$$

where Φ_{AC} is the transport of the AC and Φ_L is the leakage. Here, R measures the proportion of the AC that retroflects and is dependent on the method chosen to compute Φ_L and Φ_{AC}. This index was first introduced by Dijkstra and De Ruijter (2001), who computed the leakage with a method similar to the total transport method described in section 2b. The difference is that they computed steady states so no time averaging was applied. It was also used by Hermes et al. (2007), who deduced the leakage from the difference between the AC and Agulhas Return Current.

Here, we use the leakage computed from the Eulerian tracer method defined in section 2b. The net AC transport is computed at 32°S across a zonal section of 5° as in Fig. 1. The index R allows us to qualitatively compare our results with Dijkstra and De Ruijter (2001). The difference in our experiments is that we are not looking at steady states but at statistical equilibrium states, so the rectification effects due to instabilities are also considered. Also, the wind stress τ is the control parameter so that the relative role of the inertia increases with τ. Dijkstra and De Ruijter (2001) varied the Ekman number (i.e., eddy viscosity) and the layer depth to vary the role of inertia. In BT025, which is a similar model to the one they were using, we also observe that, for a wind increase, R is first decreasing and then increasing (Fig. 4a).

To explain this interesting result, we analyze the relative importance of advection and viscosity in the zonal momentum equation in the upper layer in the retroflection region. To investigate the importance of the nonlinearities of the flow we split the advection term into two parts,

$$\overline{h\left(\frac{u}{r_0\cos\theta}\frac{\partial u}{\partial\phi} + \frac{v}{r_0}\frac{\partial u}{\partial\theta}\right)} = \overline{h}\left(\frac{\overline{u}}{r_0\cos\theta}\frac{\partial\overline{u}}{\partial\phi} + \frac{\overline{v}}{r_0}\frac{\partial\overline{u}}{\partial\theta}\right) + F, \tag{3}$$

where the overbars are used to indicate time averages, θ is latitude, ϕ is longitude, r_0 is the radius of the earth, and (u, v) are the velocities in the zonal and meridional directions. The first two terms on the right-hand side are the advection of the mean and F represents the fluctuation terms; F is composed of eight terms and we are not interested in the details of these terms here but only in their sum. Because in the retroflection area there are regions with positive advection and regions with negative advection, we take the absolute value of each term before computing and plotting the spatial average (Fig. 5). With this method, the total advection is not equal to the advection of the mean plus the fluctuations anymore, but it gives a good indication on their average importance for the flow. We focus only on the viscosity and advection term because of their important role for the retroflection. The basic effect of the viscous boundary layer is to reduce the leakage (in the extreme case, there is viscous choking). However, the eddy viscosity is fixed so that the viscous terms become relatively unimportant for increasing wind (but still tend to reduce leakage).

For BC025, the viscosity is more important than the advection for $\tau \in [0.05, 0.2]$ N m^{-2} (Fig. 5a) because the model is still in the viscous regime and the weak retroflection is due to the high viscosity. When the wind stress increases, the relative importance of the viscosity decreases, and this leads to reduced R. On the other hand, for τ larger than $\tau = 0.2$ N m^{-2}, advection is more important than viscosity, the mechanism of the retroflection changes, and an increase of τ leads to an increase of R. This regime was called the inertial regime. In the viscous regime, the retroflection of BC025 is almost the same as that in BT025 but, for a wind stress larger than $\tau = 0.2$ N m^{-2}, R increases in the baroclinic model. This effect has already been reported by Boudra and De Ruijter (1986) and Chassignet and Boudra (1988): vortex stretching increases R and baroclinic instabilities have a dominant role in this increase because the part of the advection that is due to the fluctuations of the flow is the most important in this case (not shown).

For the high-resolution model simulations (BT01 and BC01), the variance of the leakage is important. The error E is given by $E = 1.96\sigma/\sqrt{N}$, where σ is the standard

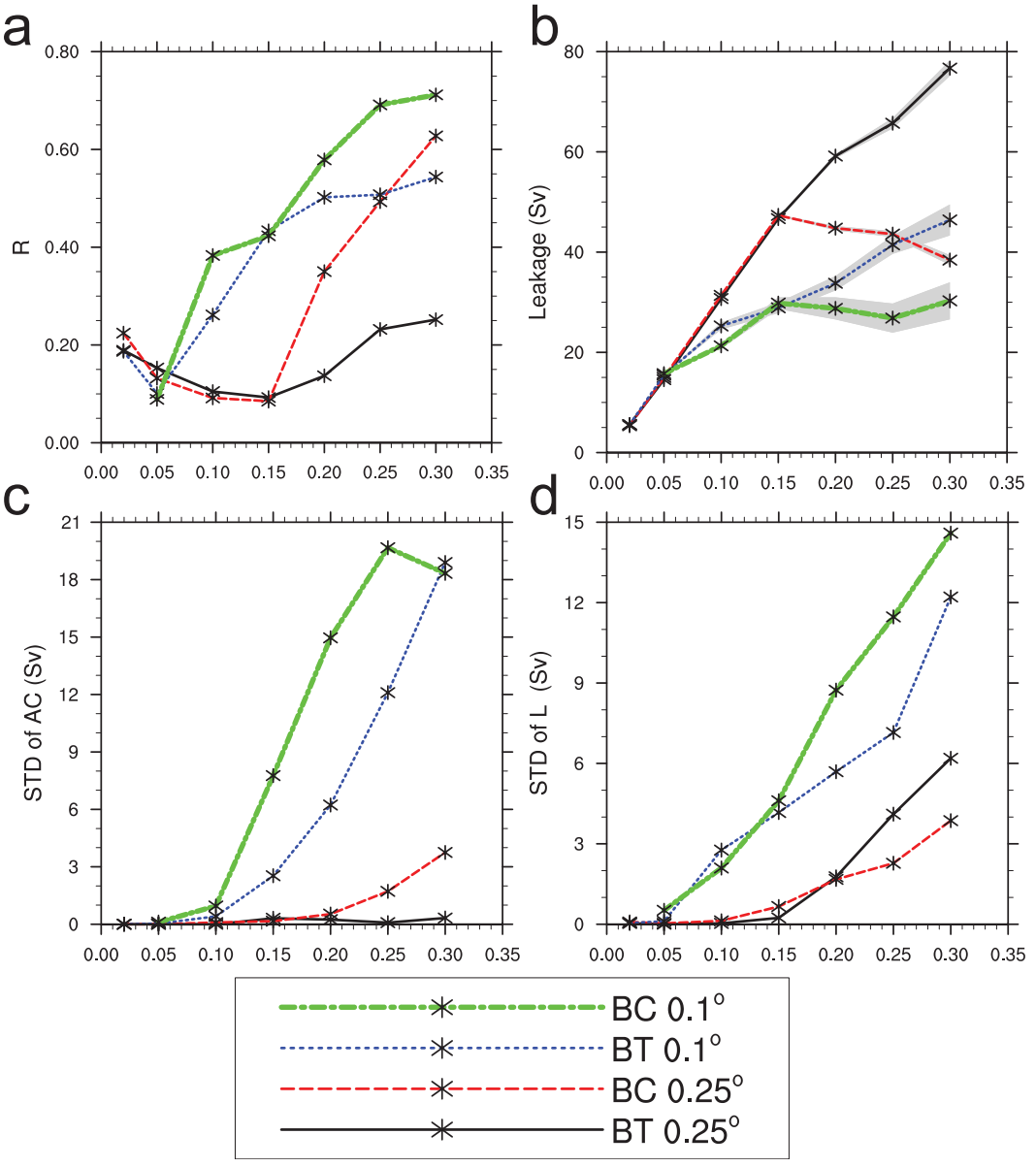

FIG. 4. (a) Retroflection index, (b) leakage with the 95% confidence intervals in gray, (c) standard deviation of the AC, and (d) of the leakage as a function of wind stress forcing.

deviation of the transport time series and N is the number of independent elements in the time series. For these time series, with monthly output, the lag-1 autocorrelation is already negative so the elements of the time series are all independent; for 5 yr, it gives $N = 60$. Assuming a normal distribution of the transport this error gives the 95% confidence interval that we indicate in Fig. 4b. These models are in the viscous regime only for weak wind forcing $\tau < 0.05$ N m^{-2} (Fig. 5b). Here, R is then increasing quickly with τ and is much more important than for intermediate-resolution models (Fig. 4a) because viscosity is smaller and inertia larger. One should be careful with the interpretation of these results: an increase of R means that a larger proportion of the AC retroflects but not necessarily that the leakage decreases. In these models, the inertial overshoot mechanism leads to an increase of R but, when the inertia is increased by increasing the volume transport of the AC, the absolute amount of leakage also increases (Fig. 4b). This increase is monotonic for BT01 but BC01 reaches a plateau at $\tau = 0.15$ N m^{-2}; after this point, all additional transport of the AC retroflects.

In the experiments with $\tau = 0.15$ N m^{-2}, the standard deviation of the AC and of the leakage become

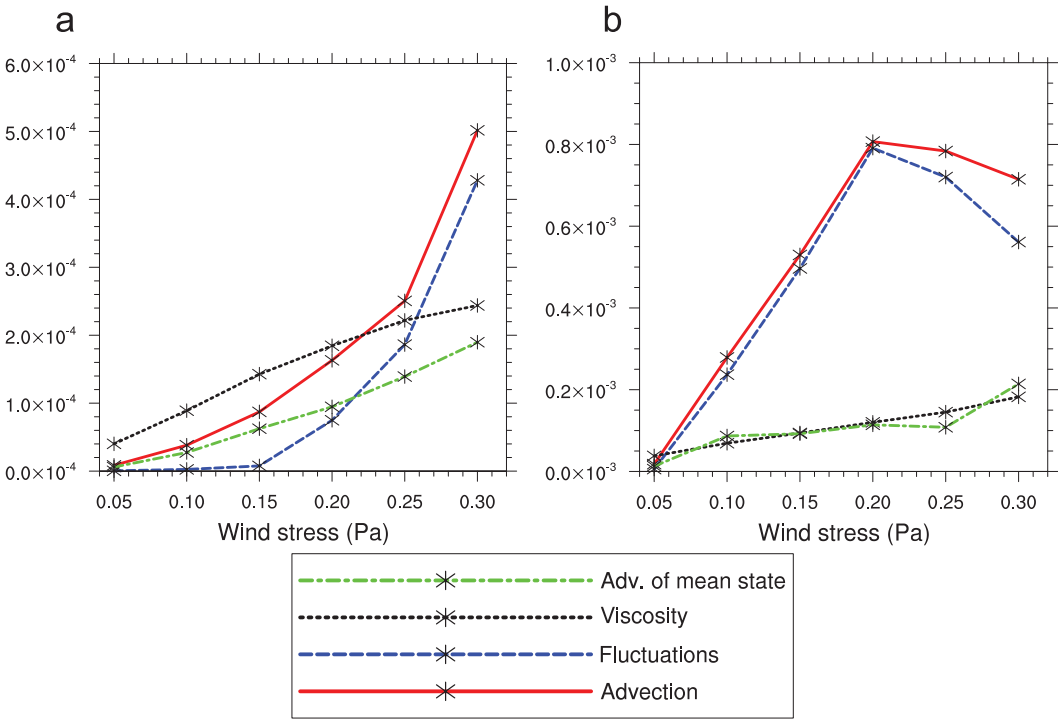

FIG. 5. Magnitude of different terms of the zonal momentum equation vertically integrated on the top layer. The average of the absolute value of each term is taken on the retroflection area (40°–36°S, 22°–30°E); unit is $m^2\ s^{-2}$. (a) BT025 and (b) BC01. The advection of the mean state and the fluctuations are the two components of the total advection [see Eq. (3)]. However, we take the absolute value of each point before averaging so here the total advection is not equal to the advection of the mean plus the fluctuations.

significant (Figs. 4c,d). Apparently, the retroflection enters another regime in which the variability of the flow becomes a dominant factor. The advection is mostly composed of fluctuations (Fig. 5b) but surprisingly less for $\tau > 0.02$ N m^{-2}. When the advection of momentum becomes dominated by the fluctuating field, westward momentum of the AC is advected southward by the fluctuating field while eastward momentum of the "South Atlantic Current" (the flow south of the retroflection) is advected northward. For increasing wind, the gradients in the flow field first increase and this advection first increases (Fig. 5b). However, the effective mixing of zonal momentum by the fluctuating field tends to reduce the gradients and thus the advection. Eventually, the effectiveness of the latter process, which may be seen as a form of "shear dispersion," is such that the growth of the mean advection stops and even shows some decrease. At this stage the mean flow field in this turbulent region hardly changes anymore, including the leakage.

In this regime, which we will call the turbulent retroflection regime, the magnitude of the AC transport does not seem to be important anymore for the amount of leakage. No more AC water can be "squeezed" through the Agulhas gateway. The sensitivity of this phenomenon to the position of the western boundary of the domain was checked with an experiment in which the domain is extended westward to 50°W. In that case, for a wind stress of $\tau = 0.2$ N m^{-2} the average leakage was somewhat smaller than in the reference experiment, 25 Sv versus 29 Sv, showing that, in the results above, the plateau is not caused by the proximity of the western boundary. The physical mechanism of the occurrence of the plateau is analyzed in section 6.

5. Position of the Agulhas Current retroflection

The main source of observations of the dynamics of the currents south of Africa is the dynamic topography measured by satellites. From these data, it is possible to deduce the position of the AC retroflection, but computing the AC transport and the leakage is not possible. An important issue is then to evaluate the possibility to find a relation between the longitudinal position of the retroflection of the AC to the AC transport and to the leakage. Methods used to determine an indicator of the longitudinal position of the retroflection loop were based on the dynamic topography field (Van Sebille et al. 2009a; Dencausse et al. 2010). Here, we base it on the volume

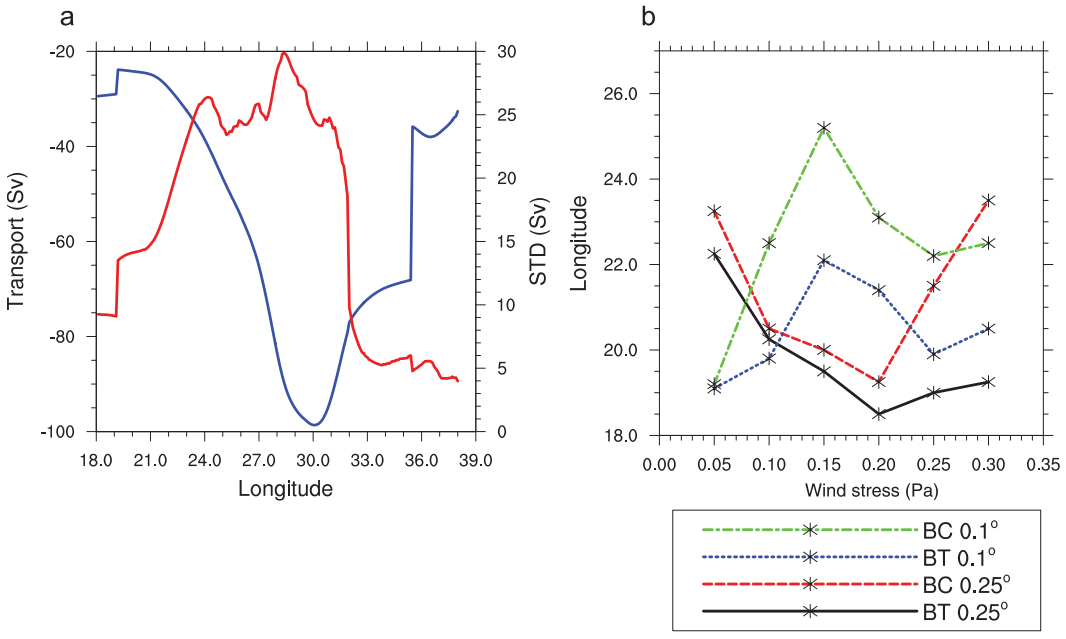

FIG. 6. (a) Transport (blue, left axis) and standard deviation (red, right axis) of the average westward flow component south of Africa for BC01 forced by a wind stress of 0.2 N m^{-2}. (b) Longitude of the 95% retroflection as a function of wind stress forcing.

transport field. The westward flow component south of the African continent is integrated for each longitude (Fig. 6a). For BC01 forced by $\tau = 0.2$ N m^{-2}, the average westward flow increases from 38° to 30°E, where its maximum strength is reached. Then it decreases from 30° to 19°E, because of both the weakening of the inertial recirculation and the retroflection. This region of recirculation–retroflection is characterized by a large standard deviation of the transport. For this configuration, it is 25 Sv at 30°E, which is 5 times that upstream (Fig. 6a). As an indicator for the mean retroflection position, we use the longitude for which 95% of the retroflection takes place east of it (Fig. 6b). We do not use the value 100%, because then the noise in the measure becomes important.

The first result is that, as for the leakage, there is no simple relation between the mean position of the retroflection and the wind stress amplitude. From the inviscid model study of Ou and De Ruijter (1986), we expect the AC to separate from the coast and to retroflect more to the east when the current has more inertia. This is what we can see in our results in the inertial regime (Fig. 6b): that is, for high values of τ in the intermediate-resolution models (BT025 and BC025) and for low values of τ for the high-resolution models (BT01 and BC01). An interesting result is that, when the retroflection is in a viscous regime (weak wind forcing of BT025 and BC025), the relation is the opposite, a stronger AC retroflects more to the west. This is consistent with the fact that the retroflection is due to the important friction in this regime. For BT01 and BC01 forced by τ superior to 0.2 N m^{-2}, there is a westward shift of the retroflection and then specially for BC01 the retroflection position is less sensitive to an increase of the wind stress.

Little evidence of a relation between position of the retroflection and leakage is available in the literature. Van Sebille et al. (2009a) found in a global model a linear correlation between leakage magnitude and westward position of the retroflection. From our set of simulations, finding a general relation between these two quantities is not possible. In fact, for two models in the same regime, BC025 under strong wind stress and BC01 under weak wind stress, an eastward shift of the retroflection leads to less and more leakage, respectively. However, the relation with the retroflection index is more straightforward. For both the viscous and the inertial regime a westward (eastward) shift of the position of the retroflection leads to a decrease (increase) of the retroflection index. In the turbulent regime, the relation is the opposite, although the variations of both the retroflection position and the retroflection index are very small.

For the BC01 configuration, Fig. 7 shows the spatial flow characteristics of the different regimes. For weak wind forcing, there is a transition between the viscous and the inertial regime: only a small part of the AC retroflects and the flow is almost steady (Fig. 7a). For stronger wind, the retroflection appears and the EKE is important in the

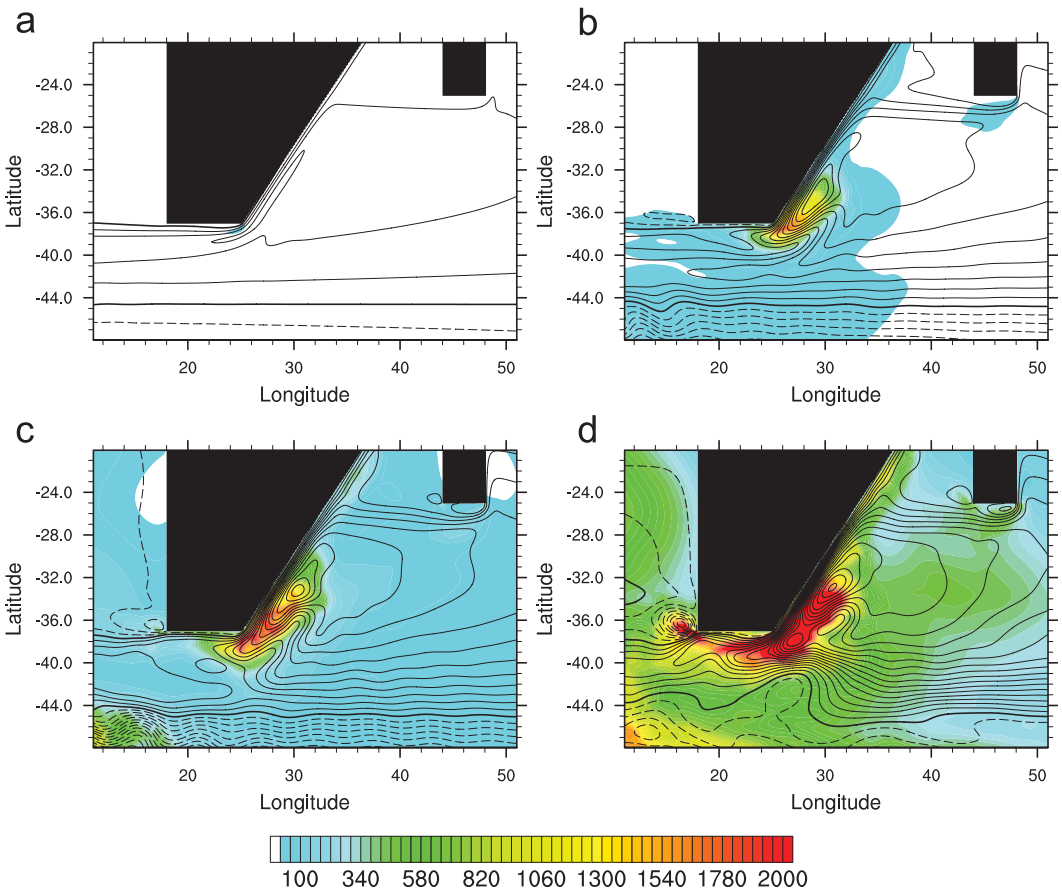

FIG. 7. Zoom on the AC retroflection for BC01 forced by a wind stress of (a) 0.05, (b) 0.15, (c) 0.2, and (d) 0.3 N m^{-2}. Lines are contours of sea surface height every 5 cm, and colors represent the EKE (cm^2 s^{-2}).

retroflection region; this is the inertial regime (Fig. 7b). For larger wind stress, the retroflection position spreads over a larger area and the EKE increases; this is the transition between the inertial and the turbulent regime (Fig. 7c). Finally, for strong wind forcing, the retroflection area is large and the average leakage is limited to a narrow flow ($\simeq$100 km) south of the African continent (Fig. 7d).

The dynamical relations between wind stress, AC transport, retroflection position, retroflection index, and leakage in the three regimes defined here (viscous, inertial, and turbulent) are summarized in Table 2. To determine these qualitative relations, the intermediate-resolution models (BT025 and BC025) were used for the viscous regime and the high-resolution models (BT01 and BC01) were used for the inertial and turbulent regimes.

6. Turbulent regime

As shown in section 4, the new regime appears when the variability of the flow becomes important. It is then likely that the impact of the variability on the statistical steady state gives an indication on the physical mechanism at the origin of the plateau of the leakage. We therefore compute the fluctuations of the tracer flux in the zonal and the meridional directions,

$$\overline{UC} = \overline{U}\,\overline{C} + \overline{U'C'}; \quad \overline{VC} = \overline{V}\,\overline{C} + \overline{V'C'}, \qquad (4)$$

where U and V are the zonal or meridional volume transport, respectively, and C is the tracer concentration, with $U = \overline{U} + U'$, $V = \overline{V} + V'$, and $C = \overline{C} + C'$. The terms

TABLE 2. Summary of the behavior of the retroflection depending on the regime.

	Viscous	Inertial	Turbulent
AC transport	Increase	Increase	Increase
Retroflection position	Westward	Eastward	Westward
Retroflection index	Decrease	Increase	Increase
Leakage	Increase	Increase	Constant
		τ increase →	

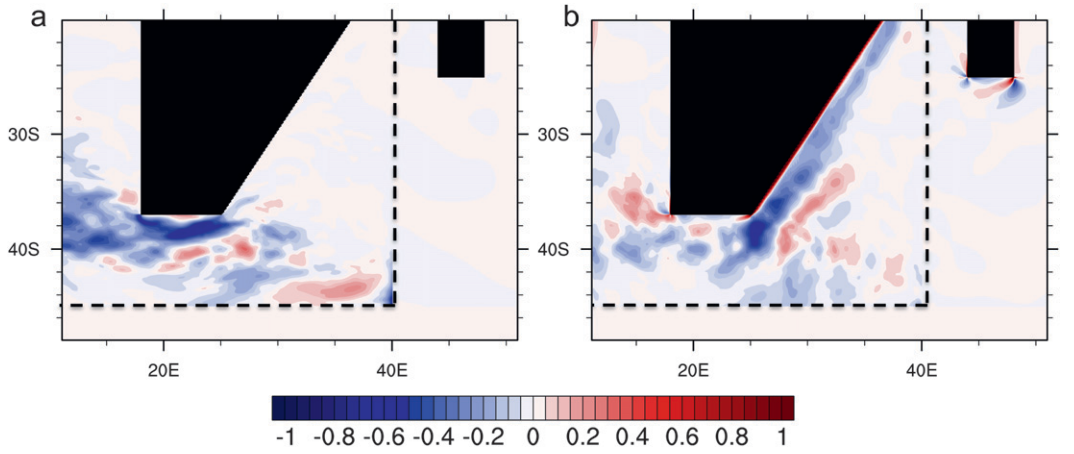

FIG. 8. Rectified part of the volume flux of tracer (Sv) in (a) zonal and (b) meridional directions for simulation BC01 forced by a wind stress of 0.3 N m^{-2}, corresponding to the terms $\overline{U'C'}$ and $\overline{V'C'}$ of Eq. (4). Unit is given in Sverdrups for each model grid cell; see the text for integrated transport magnitude. The dashed lines indicate the limit of the area in which the value of the tracer can evolve freely.

$\overline{U'C'}$ and $\overline{V'C'}$ in Eq. (4) represent a rectified effect that becomes important for strongly turbulent flows.

A map of the rectification terms shows that the term $\overline{U'C'}$ has the impact of increasing the leakage (Fig. 8a). Meridional integration of the flux at 12°E shows a magnitude of 22 Sv, which represents most of the total flux of 26 Sv (see Fig. 9a). It is then unlikely that this term is at the origin of the plateau reached by the leakage in the turbulent regime. On the other hand, the meridional rectification term shows a southward flux of tracer across

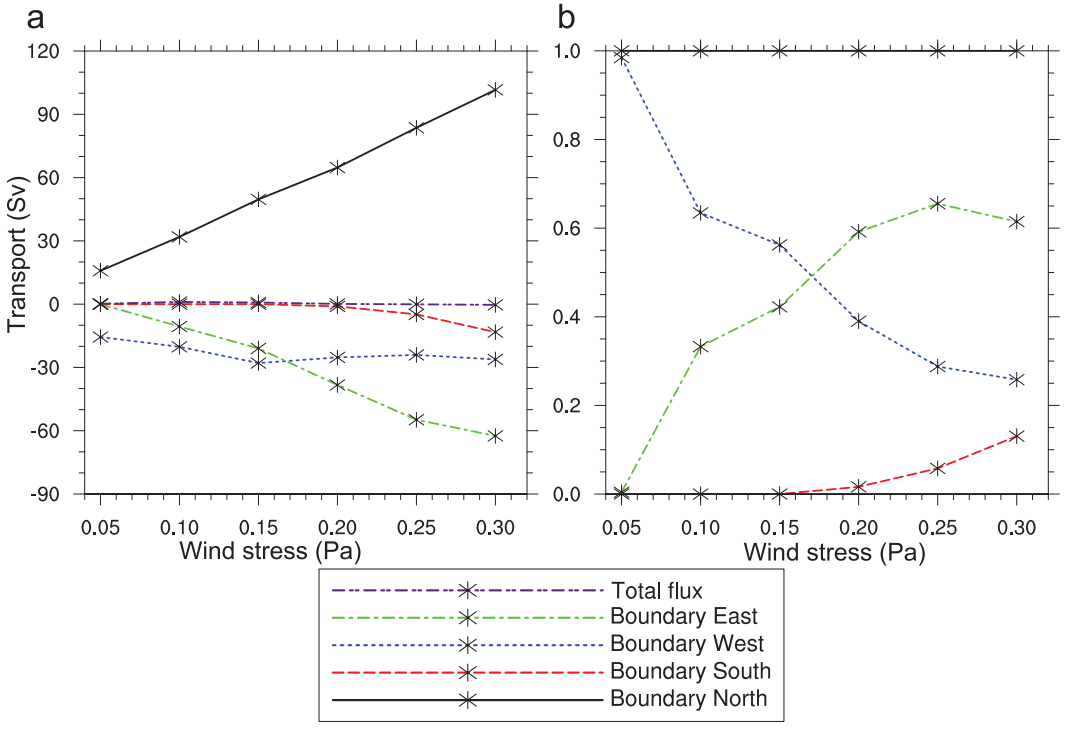

FIG. 9. (a) Mean volume flux of Indian Ocean tracer entering a box (see Fig. 1) as a function of wind stress forcing and (b) absolute value of the transport through the eastern, southern, and western boundaries divided by the transport of the northern boundary for simulation BC01.

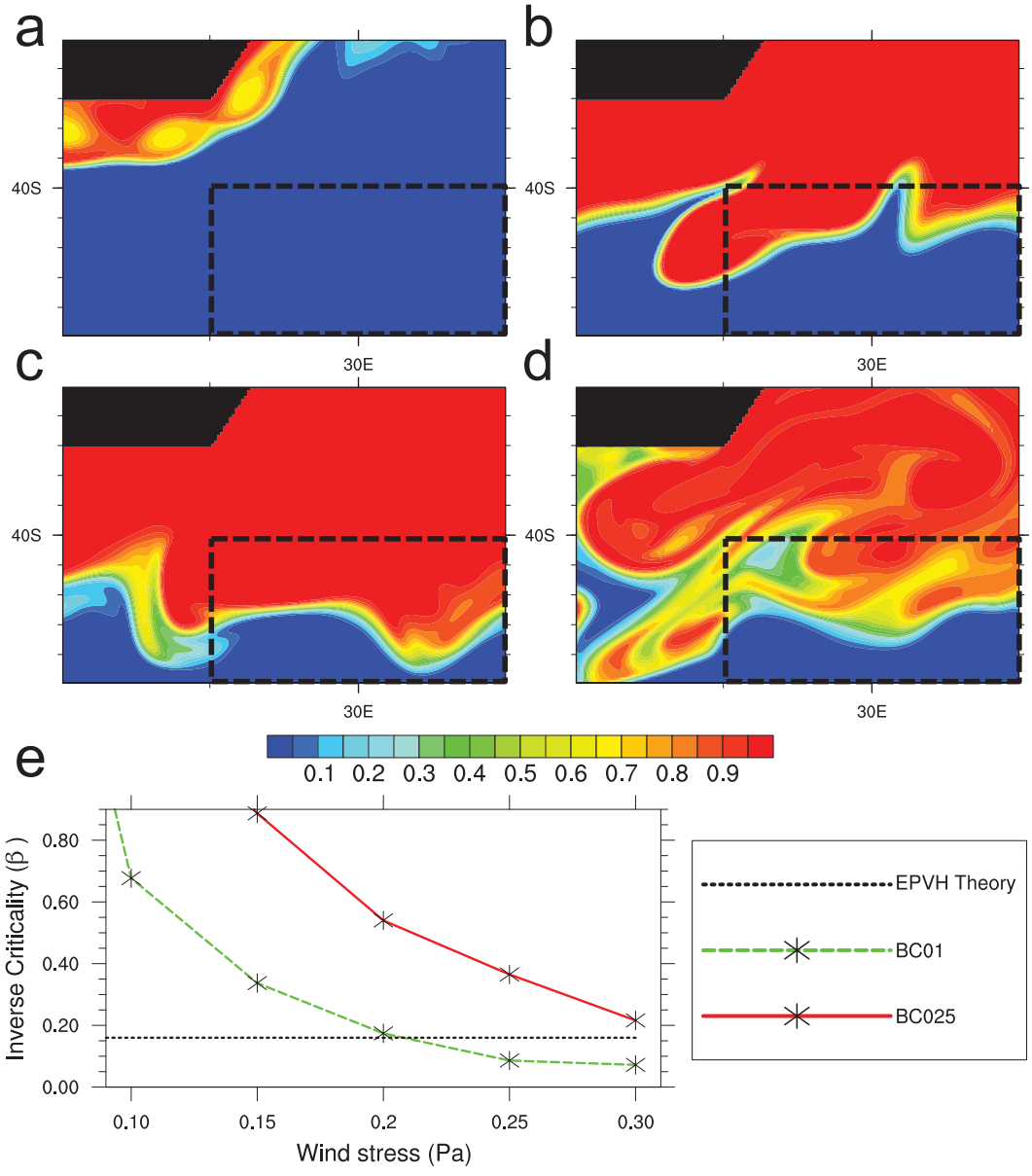

FIG. 10. Snapshots of tracer concentration for BC01 forced by a wind stress of (a) 0.05, (b) 0.15, (c) 0.2, and (d) 0.3 N m^{-2}. (e) Spatial average of the inverse criticality in the box shown in (a)–(d) as a function wind stress.

42°–45°S, 25°–35°E (Fig. 8b). The magnitude of this term integrated zonally at 45°S is 13 Sv, which is equal to the total southward transport at this latitude. This is a confirmation of what we can already guess from the SSH pattern on Fig. 7d: there is no southward flow in the mean state at this latitude. It represents a flux of tracer that leaves the box without contributing to the leakage. In fact, if we look at the tracer fluxes through the boundaries of a box south of the African continent (Fig. 9), the southward flux at 45°S becomes significant for τ larger than 0.2 N m^{-2} when the turbulent retroflection regime is entered. This flux then quickly increases because of eddy rectification and reaches 13 Sv for $\tau = 0.3$ N m^{-2}.

The position of the front between Indian Ocean waters and the Antarctic Circumpolar Current can be visualized with snapshots of the tracer concentration (Fig. 10). For weak wind, the front is very well delimited and acts as a transport barrier (Figs. 10a,b), but when the wind stress increases this barrier breaks up and from $\tau = 0.2$ N m^{-2} there is mixing between the water masses. A theory to predict the equilibration of turbulent baroclinic jets in quasigeostrophic two-layer models was developed by

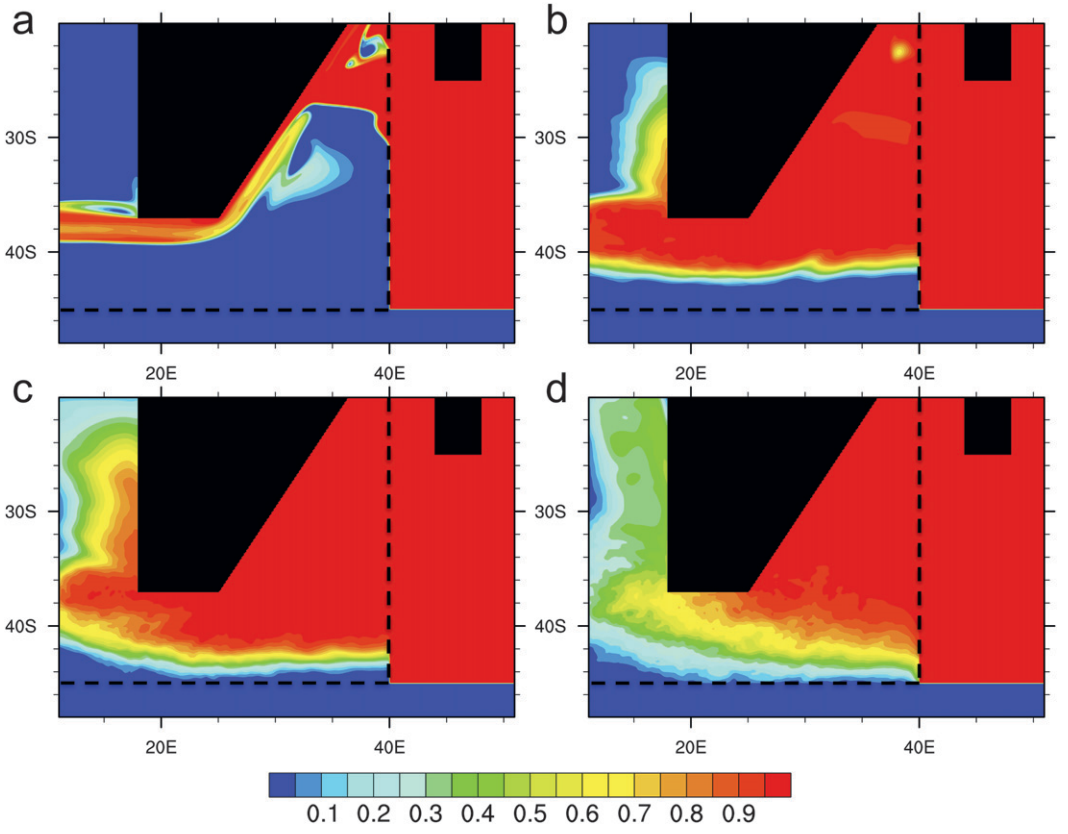

FIG. 11. Mean tracer concentration for a wind stress of (a) 0.05, (b) 0.15, (c) 0.2, and (d) 0.3 N m^{-2} for simulation BC01. The dashed lines indicate the limit of the area in which the value of the tracer can evolve freely.

Esler (2008b). This equilibration via PV homogenization (EPVH) theory is based on the hypothesis that the eddy field forces the mean flow toward a final state that has the minimum possible potential energy. Esler (2008a) extended the EPVH theory to predict whether a baroclinically unstable eastward flow is a robust transport barrier. To compare our results with this theory, we compute the inverse criticality β that is a measure of the degree of instability of the jet,

$$\beta = \frac{\beta^* L_D^2}{u}, \tag{5}$$

where β^* is the latitudinal gradient of Coriolis acceleration; u is the zonal velocity; and $L_D = \sqrt{g'h/2f^2}$ is the internal Rossby radius of deformation, with g' being the reduced gravity at the interface between the two layers, h being the upper-layer depth and f being the Coriolis parameter. We compute β in the Agulhas Return Current using instantaneous fields of u and h. For each model grid point, we take the minimum β reached during the simulation and we average spatially over a box (Fig. 10). We compare the value of β in the results of BC01 and BC025 with the theoretical value ($\beta = 0.16$) for which the jet is expected to enter the ''leaky'' regime (Fig. 10e). We see that the theoretical prediction is in accordance with what we observed from snapshots of the front (Fig. 10c). The inverse criticality decreases when the wind stress increases and, for $\tau = 0.2$ N m^{-2} when cross-jet exchange starts in BC01, the model reaches a value very close to the theoretical value for the regime shift (Esler 2008a). The change of character of the front and the associated increase in cross-jet transport of tracer leads to a decrease of the tracer concentration south of the African continent (Fig. 11), which tends to decrease the mean westward tracer transport [cf. Eq. (4)].

7. Summary and conclusions

The Agulhas Current retroflection is an intriguing flow system. We have studied the retroflection dynamics here in an idealized Indian Ocean model with barotropic and baroclinic shallow-water models of intermediate and very high resolution. In this way, the study generalizes many results of earlier idealized

models (Chassignet and Boudra 1988; Dijkstra and De Ruijter 2001). In this study, we focused on the importance of the wind stress strength at a fixed pattern for the AC leakage. Sensitivity studies on the importance of the wind stress pattern and particularly of the meridional location of the zero wind stress curl are outside the scope of this paper.

Although the relation between the volume transport of the main currents of the Indian Ocean and the wind stress curl magnitude is almost linear, the dynamics of the leakage is much more complex. The main new result in this paper is that three regimes of retroflection are identified in the simulations. The viscous regime and the inertial regime were identified earlier (De Ruijter 1982; Dijkstra and De Ruijter 2001), but we here find a new turbulent regime that appears for strong (but realistic) wind forcing in the high-resolution baroclinic versions of our ocean model. In the turbulent regime, a surprising result is that the magnitude of the leakage reaches a plateau at a value of approximately 30 Sv. It is explained by the fact that, because of the instability of the Agulhas Return Current, a significant part of the water from the Indian Ocean is advected southward in the Antarctic Circumpolar Current. This breaking up of the front between the Indian Ocean waters and the northern part of the Antarctic Circumpolar Current happens for a value of the inverse criticality parameter predicted by the EPVH theory (Esler 2008a). The volume of Indian Ocean water south of Africa is decreased, and the leakage to the Atlantic reaches a limit. This leads to a decorrelation between the wind stress magnitude and the leakage and similarly between the AC transport computed across a large zonal section and the leakage.

The sensitivity of the models to horizontal resolution, viscosity, and baroclinic effects shows that any model result of the Agulhas System has to be interpreted carefully. To our knowledge, convergence of model results with respect to resolution has not been demonstrated for any ocean model. On the other hand, we do not expect that a resolution higher than 0.1° could lead to very different results, because we already resolve the Rossby deformation radius that is of 44 km at 60°S.

Satellite observations of the dynamic topography suggest that the south Subtropical Front, which marks the southern limit of subtropical waters, is continuous in the mean but is often disrupted by eddies at smaller time scales (Dencausse et al. 2011). This is an indication for the relevance of the physical mechanism highlighted in this paper for the real ocean. However, further research would be necessary to assess the quantitative importance of cross-jet transport in the Agulhas Return Current, as it is done for the Gulf Stream, for example, using observations of drifters (Bower and Lozier 1994; Brambilla and Talley 2006) or advection of numerical drifters using observations of velocities (Rypina et al. 2011).

Acknowledgments. The authors are funded by the Netherlands Organization for Scientific Research through the INATEX program, ZKO 839.08.430. We thank Michael Kliphuis (IMAU-UU) for his assistance in carrying out the numerical computations with the HIM.

REFERENCES

Beal, L. M., W. P. M. De Ruijter, A. Biastoch, and R. Zahn, 2011: On the role of the Agulhas system in ocean circulation and climate. *Nature,* **472,** 429–436.

Biastoch, A., C. W. Böning, and J. R. E. Lutjeharms, 2008: Agulhas leakage dynamics affects decadal variability in Atlantic overturning circulation. *Nature,* **456,** 489–492, doi:10.1038/nature07426.

Boudra, D. B., and W. P. M. De Ruijter, 1986: The wind-driven circulation in the South Atlantic-Indian Ocean—II. Experiments using a multi-layer numerical model. *Deep-Sea Res.,* **33,** 447–482.

Bower, A. S., and M. S. Lozier, 1994: A closer look at particle exchange in the Gulf Stream. *J. Phys. Oceanogr.,* **24,** 1399–1418.

Brambilla, E., and L. D. Talley, 2006: Surface drifter exchange between the North Atlantic subtropical and subpolar gyres. *J. Geophys. Res.,* **111,** C07026, doi:10.1029/2005JC003146.

Chassignet, E. P., and D. B. Boudra, 1988: Dynamics of Agulhas Retroflection and ring formation in a numerical model. Part II: Energetics and ring formation. *J. Phys. Oceanogr.,* **18,** 304–319.

Dencausse, G., M. Arhan, and S. Speich, 2010: Spatio-temporal characteristics of the Agulhas Current retroflection. *Deep-Sea Res. I,* **57,** 1392–1405.

——, ——, and ——, 2011: Is there a continuous subtropical front south of Africa? *J. Geophys. Res.,* **116,** C02027, doi:10.1029/2010JC006587.

De Ruijter, W. P. M., 1982: Asymptotic analysis of the Agulhas and Brazil Current systems. *J. Phys. Oceanogr.,* **12,** 361–373.

——, A. Biastoch, S. S. Drijfhout, J. R. E. Lutjeharms, R. P. Matano, T. Pichevin, P. J. Van Leeuwen, and W. Weijer, 1999: Indian-Atlantic interocean exchange: Dynamics, estimation and impact. *J. Geophys. Res.,* **104** (C9), 20 885–20 910.

Dijkstra, H. A., and W. P. M. De Ruijter, 2001: On the physics of the Agulhas Current: Steady retroflection regimes. *J. Phys. Oceanogr.,* **31,** 2971–2985.

Easter, R. C., 1993: Two modified versions of Bott's positive-definite numerical advection scheme. *Mon. Wea. Rev.,* **121,** 297–304.

Esler, J. G., 2008a: Robust and leaky transport barriers in unstable baroclinic flows. *Phys. Fluids,* **20,** 116602, doi:10.1063/1.3013631.

——, 2008b: The turbulent equilibration of an unstable baroclinic jet. *J. Fluid Mech.,* **599,** 241–268.

Godfrey, J. S., 1989: A Sverdrup model of the depth-integrated flow for the World Ocean allowing for island circulations. *Geophys. Astrophys. Fluid Dyn.,* **45,** 89–112.

Gordon, A. L., 1986: Interocean exchange of thermocline water. *J. Geophys. Res.,* **91** (C4), 5037–5046.

Hallberg, R., 1997: Stable split time stepping schemes for large-scale ocean modeling. *J. Comput. Phys.,* **135,** 54–65.

Hermes, J. C., C. J. C. Reason, and J. R. E. Lutjeharms, 2007: Modeling the variability of the greater Agulhas Current system. *J. Climate,* **20,** 3131–3146.

Ou, H. W., and W. P. M. De Ruijter, 1986: Separation of an inertial boundary current from a curved coastline. *J. Phys. Oceanogr.,* **16,** 280–289.

Penven, P., S. Herbette, and M. Rouault, 2011: Ocean modelling in the Agulhas Current system. *Proc. Nansen-Tutu Conf.,* Cape Town, South Africa, Nansen-Tutu Centre for Marine Environmental Research.

Risien, C. M., and D. B. Chelton, 2008: A global climatology of surface wind and wind stress fields from eight years of QuikSCAT scatterometer data. *J. Phys. Oceanogr.,* **38,** 2379–2413.

Rouault, M., P. Penven, and B. Pohl, 2009: Warming in the Agulhas Current system since the 1980's. *Geophys. Res. Lett.,* **36,** L12602, doi:10.1029/2009GL037987.

Rypina, I. I., L. J. Pratt, and M. S. Lozier, 2011: Near-surface transport pathways in the North Atlantic Ocean: Looking for throughput from the subtropical to the subpolar gyre. *J. Phys. Oceanogr.,* **41,** 911–925.

Schmitz, W. J., Jr., 1996: On the eddy field in the Agulhas Retroflection, with some global considerations. *J. Geophys. Res.,* **101** (C7), 16 259–16 271.

Sprintall, J., S. Wijffels, R. Molcard, and I. Jaya, 2009: Direct estimates of the Indonesian Throughflow entering the Indian Ocean: 2004–2006. *J. Geophys. Res.,* **114,** C07001, doi:10.1029/2008JC005257.

Van Sebille, E., C. N. Barron, A. Biastoch, P. J. van Leeuwen, F. C. Vossepoel, and W. P. M. de Ruijter, 2009a: Relating Agulhas leakage to the Agulhas Current retroflection location. *Ocean Sci.,* **5,** 511–521, doi:10.5194/os-5-511-2009.

——, A. Biastoch, P. J. Van Leeuwen, and W. P. M. De Ruijter, 2009b: A weaker Agulhas Current leads to more Agulhas leakage. *Geophys. Res. Lett.,* **36,** L03601, doi:10.1029/2008GL036614.

Weijer, W., W. P. M. De Ruijter, A. Sterl, and S. S. Drijfhout, 2002: Response of the Atlantic overturning circulation to South Atlantic sources of buoyancy. *Global Planet. Change,* **34,** 293–311.